Geophysical Journal International

Geophys. J. Int. (2012) **189,** 999–1014 doi: 10.1111/j.1365-246X.2012.05377.x

Source parameters of microearthquakes on an interplate asperity off Kamaishi, NE Japan over two earthquake cycles

Naoki Uchida,[1] Toru Matsuzawa,[1] William L. Ellsworth,[2] Kazutoshi Imanishi,[3] Kouhei Shimamura,[1] and Akira Hasegawa[1]

[1] *Research Center for Prediction of Earthquakes and Volcanic Eruptions, Graduate School of Science, Tohoku University, Sendai* 980-8578*, Japan. E-mail: uchida@aob.gp.tohoku.ac.jp*

[2] *U. S. Geological Survey, Menlo Park, CA* 94025*, USA*

[3] *Geological Survey of Japan, AIST, Tsukuba Central* 7 1-1*, Higashi* 1 *Tsukuba, Ibaraki-ken* 305-8567*, Japan*

Accepted 2012 January 9. Received 2011 December 28; in original form 2011 June 8

SUMMARY

We have estimated the source parameters of interplate earthquakes in an earthquake cluster off Kamaishi, NE Japan over two cycles of $M \sim 4.9$ repeating earthquakes. The $M \sim 4.9$ earthquake sequence is composed of nine events that occurred since 1957 which have a strong periodicity (5.5 ± 0.7 yr) and constant size ($M4.9 \pm 0.2$), probably due to stable sliding around the source area (asperity). Using *P*- and *S*-wave traveltime differentials estimated from waveform cross-spectra, three $M \sim 4.9$ main shocks and 50 accompanying microearthquakes ($M1.5$–3.6) from 1995 to 2008 were precisely relocated. The source sizes, stress drops and slip amounts for earthquakes of $M2.4$ or larger were also estimated from corner frequencies and seismic moments using simultaneous inversion of stacked spectral ratios. Relocation using the double-difference method shows that the slip area of the 2008 $M \sim 4.9$ main shock is co-located with those of the 1995 and 2001 $M \sim 4.9$ main shocks. Four groups of microearthquake clusters are located in and around the mainshock slip areas. Of these, two clusters are located at the deeper and shallower edge of the slip areas and most of these microearthquakes occurred repeatedly in the interseismic period. Two other clusters located near the centre of the mainshock source areas are not as active as the clusters near the edge. The occurrence of these earthquakes is limited to the latter half of the earthquake cycles of the $M \sim 4.9$ main shock. Similar spatial and temporal features of microearthquake occurrence were seen for two other cycles before the 1995 $M5.0$ and 1990 $M5.0$ main shocks based on group identification by waveform similarities. Stress drops of microearthquakes are 3–11 MPa and are relatively constant within each group during the two earthquake cycles. The 2001 and 2008 $M \sim 4.9$ earthquakes have larger stress drops of 41 and 27 MPa, respectively. These results show that the stress drop is probably determined by the fault properties and does not change much for earthquakes rupturing in the same area. The occurrence of microearthquakes in the interseismic period suggests the intrusion of aseismic slip, causing a loading of these patches. We also found that some earthquakes near the centre of the mainshock source area occurred just after the earthquakes at the deeper edge of the mainshock source area. These seismic activities probably indicate episodic aseismic slip migrating from the deeper regions in the mainshock asperity to its centre during interseismic periods. Comparison of the source parameters for the 2001 and 2008 main shocks shows that the seismic moments (1.04×10^{16} Nm and 1.12×10^{16} Nm for the 2008 and 2001 earthquakes, respectively) and source sizes (radius = 570 m and 540 m for the 2008 and 2001 earthquakes, respectively) are comparable. Based on careful phase identification and hypocentre relocation by constraining the hypocentres of other small earthquakes to their precisely located centroids, we found that the hypocentres of the 2001 and 2008 $M \sim 4.9$ events are located in the southeastern part of the mainshock source area. This location does not correspond to either episodic slip area or hypocentres of small earthquakes that occurred during the earthquake cycle.

Key words: Earthquake source observations; Earthquake interaction, forecasting, and prediction; Seismicity and tectonics; Subduction zone processes; Dynamics and mechanics of faulting; Dynamics: seismotectonics.

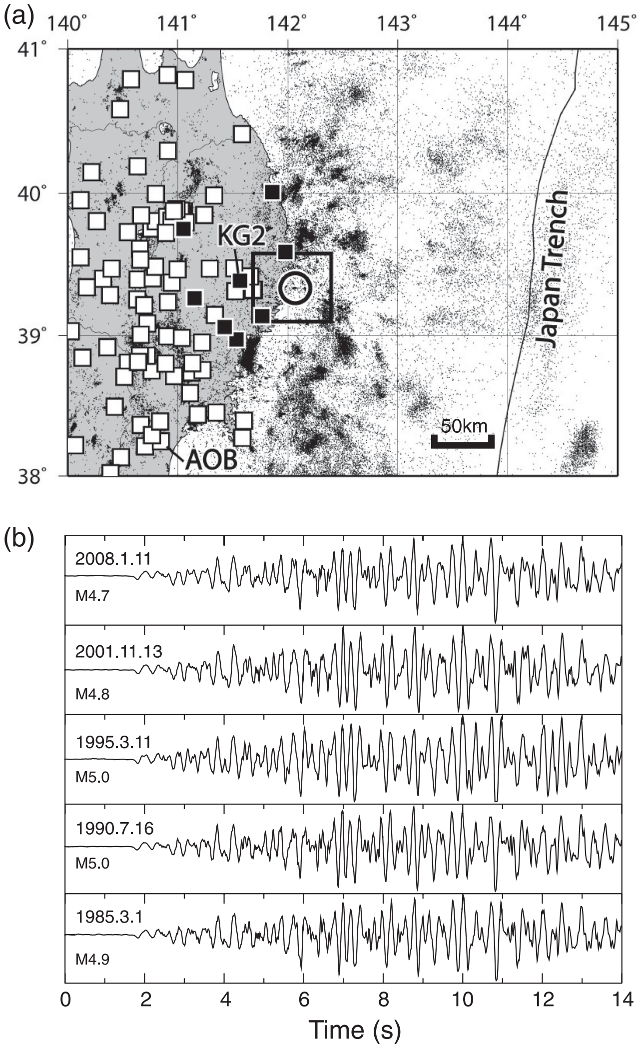

Figure 1. (a) Distribution of microearthquakes (dots) and location of off-Kamaishi earthquake cluster (circle). Shallow earthquakes (depth ≤70 km) from 1995 to 2009 January from Japan Meteorological Agency's catalogue are plotted here. White and black squares denote seismic stations used for hypocentre relocation by double-difference method (Waldhauser & Ellsworth 2000) and seismic stations used for the analysis of spectral ratios. (b) Vertical velocity seismograms of off-Kamaishi sequence recorded at AOB station shown in Panel (a). The natural period of the seismometre is 5 s. The each trace is scaled to its maximum amplitude.

1 INTRODUCTION

The well-studied off-Kamaishi repeating earthquake sequence occurred on a subduction plate boundary off the coast of Sanriku, NE Japan (Fig. 1a). Although the earthquakes are moderate in size ($M \sim 4.9$), due to a fast plate convergence rate of about 8 cm yr^{-1} they take place frequently on the asperity, with a recurrence interval of about 5 yr. This means that high-quality data are available that are usually difficult to obtain for earthquake cycle research. The sequence was first identified in 1999 (Matsuzawa *et al*. 2002) and has been intensively studied to determine its recurrence properties (Matsuzawa *et al*. 2002; Okada *et al*. 2003; Uchida *et al*. 2005, 2007). The earthquake sequence was recognized by source relocation and waveform similarity studies (Fig. 1b). It is unique in that the individual earthquakes have an almost identical magnitude ($M4.9 \pm 0.2$) and recurrence intervals (5.5 ± 0.7 yr). This is thought to be a consequence of stable sliding at the plate boundary around the asperity (∼50 km in depth) of the sequence (Matsuzawa *et al*. 2002; Uchida *et al*. 2005). The epicentre of the 2011 off the Pacific coast of Tohoku earthquake ($M9.0$) is located about 150 km southeast of the Kamaishi sequence and the Kamaishi sequence is located outside of the main slip area of the 2011 earthquake (e.g. Ide *et al*. 2011; Politz *et al*. 2011; Iinuma *et al*. 2012). The combination of simple recurrence behaviour and the availability of high-quality data makes this sequence an ideal target for investigating earthquake cycles and, in particular, the seismicity in the interseismic period. After the sequence was recognized, co-location of the slip areas for the 1995 ($M5.0$) and 2001 ($M4.8$) events was determined from waveform modelling (Okada *et al*. 2003). The effects of variations of the quasi-static slip rate on the recurrence interval were also estimated from the cumulative slip of small repeating earthquakes in the area surrounding the earthquake sequence (Uchida *et al*. 2005).

Recently, the hierarchical structure of asperities for the off-Kamaishi earthquake sequence has been revealed based on the source parameters of the 2001 earthquake and its accompanying microearthquakes (Uchida *et al*. 2007). The evolution of microearthquake activity in the earthquake cluster from low-level activity after the main shocks to higher levels during the latter halves of the cycles was discussed based on the spatio-temporal distribution of precisely located earthquakes.

On January 11, 2008, a $M4.7$ earthquake occurred in the cluster (Fig. 1b, Fig. 2), after an interval of 6.16 yr from the 2001 event. The timing of this earthquake was predicted with a 99 per cent probability based on eight recurrence intervals from 1957 to 2001 and assuming that the intervals followed a normal distribution (Matsuzawa *et al*. 2002). In this study, we show that the 2008 earthquake is a member of the $M \sim 4.9$ off-Kamaishi repeating earthquake sequence and investigate the seismic activity on the asperity over two earthquake cycles.

2 DATA AND DEFINITION OF THE OFF-KAMAISHI EARTHQUAKE CLUSTER

We use waveform and phase data from the microearthquake observation network of the Research Center for Prediction of Earthquakes and Volcanic Eruptions (RCPEV), Tohoku University, that covers the Tohoku region in Japan (Hasegawa *et al*. 1978). Most of the seismometres are 1-Hz velocity-type instruments and are installed in horizontal vaults (tunnels) about 50 m in length or in boreholes with depths of 300–500 m (Research Center for Prediction of Earthquakes and Volcanic Eruptions 2004). This network had the highest sensitivity to small earthquakes off Kamaishi until October, 1997, when the data from the network were unified with data recorded by the Japan Meteorological Agency (JMA). Digital seismograms of 100 Hz sampling have been recorded and stored since 1984, as shown in Fig. 1(b), and the dynamic range of the recordings and the number of stations increased in the 1990s. The nearest seismic station is located within 30 km in the epicentral distance (Fig. 1a).

Epicentre distribution of the earthquakes in the off-Kamaishi region (rectangle in Fig. 1a) is shown in Fig. 2(a). Taking account of earthquake detectability, RCPEV phase readings are used from 1975 to 2003 April and the JMA phase readings are used from 2003 April to 2009 January. This relocation was performed to obtain a uniform earthquake catalogue from 1975 to 2009 because original RCPEV and JMA earthquake catalogues has systematic shift due to different velocity structure model used for the hypocentre location.

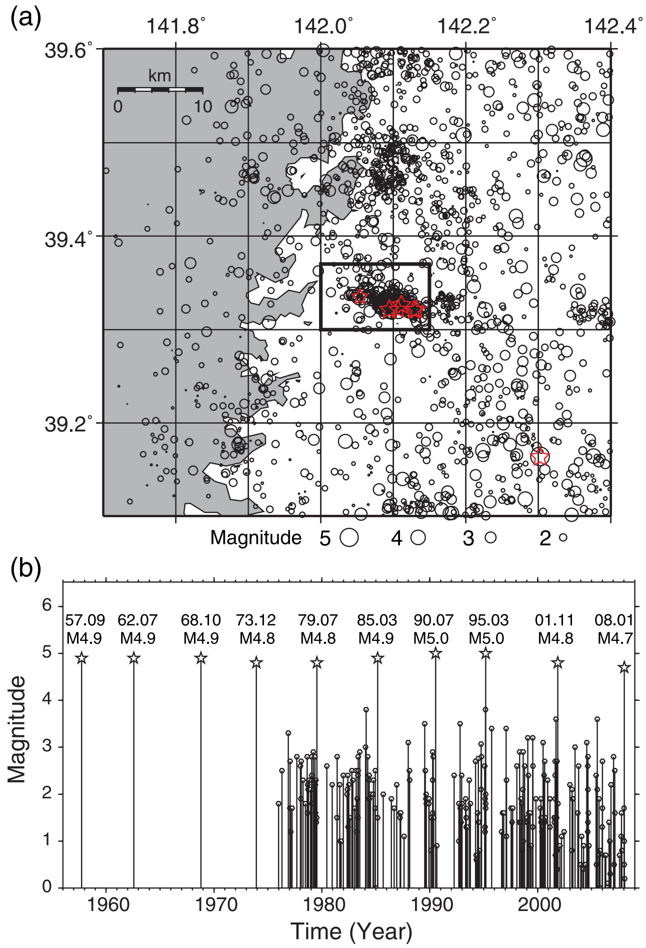

Figure 2. (a) Distribution of relocated earthquakes at off-Kamaishi region (rectangle in Fig. 1a) using Tohoku University's routing procedure (Hasegawa *et al*. 1978) for the period from 1975 to 2009 January. The depth range of the earthquake is from 35 to 60 km, near the plate boundary in this region. Earthquakes magnitudes are derived from JMA's catalogue if available and others are from RCPEV's catalogue. The symbol size is proportional to magnitude and the scale is shown at the bottom of the figure and earthquakes with M4.7 or larger are shown by red stars. See the main text for details of the relocation procedure. (b) Magnitude–time plot of earthquakes in the rectangle shown in (a). Members of the $M \sim 4.9$ sequence are indicated by stars. The $M \sim 4.9$ sequence members before 1973 are added based on Matsuzawa *et al*. (2002). JMA reports both displacement and velocity magnitudes for the large events and we adopted the displacement magnitude for all members of the $M \sim 4.9$ sequence to allow a size comparison.

We relocated these earthquakes using the 1-D velocity structure of the routine earthquake location procedure of the RCPEV (Hasegawa *et al*. 1978). Here, we used data only from stations located on land and within 200 km of the source area because data from fiber-cabled ocean bottom stations were only available after 1996 (Okada *et al*. 2004), and stations far from the source area recorded only large earthquakes. These restrictions are because the use of different stations sometimes causes shift of hypocentres due to effect of unmodelled velocity heterogeneity.

The off-Kamaishi earthquake cluster identified by this relocation procedure (rectangle in Fig. 2a) is clearly distinguishable from other seismicity in this region. Six $M \geq 4.7$ earthquakes (red circles in Fig. 2a) are located in this rectangle. The magnitude–time diagram for the earthquake cluster is shown in Fig. 2(b). The star symbols indicate periodic, similarly sized $M \sim 4.9$ main shocks that are shown in red in Fig. 2(a) and about one magnitude larger than other microearthquakes in the cluster. The waveforms recorded at the AOB station (Fig. 1b, $\Delta = 160$ km) indicates that the 2008 $M \sim 4.9$ earthquake was very similar to previous $M \sim 4.9$ repeating earthquakes, suggesting that it is also a member of the $M \sim 4.9$ sequence. Fig. 2(b) also shows that the seismicity is low just after the $M \sim 4.9$ main shocks and increases particularly in the latter half of the earthquake cycle.

3 EARTHQUAKE RELOCATION

We relocated the $M \sim 4.9$ sequence and accompanying small earthquakes in the earthquake cluster from 1995 to 2008. To clarify the process occurring during the interseismic period, we investigated the relationship between the mainshock sequence and the accompanying microearthquakes over two earthquake cycles.

To obtain better relative locations for earthquakes in the cluster, we relocated these earthquakes using the double-difference method (Waldhauser & Ellsworth 2000) with almost the same procedure as that reported by Uchida *et al*. (2007). We measured traveltime differences using the cross-spectrum method of Poupinet *et al*. (1984) for both P and S waves. The time window was set to be 3.55 s starting 1 s before the onset of each wave and the traveltime differences were estimated from the phases of cross spectra in the frequency band of 1–10 Hz with a squared coherence of greater than 0.8.

We obtained 20 089 and 14 382 traveltime differential measurements for P- and S-phases, respectively, for 53 events that occurred from 1995 to 2008 and had magnitudes in the range 1.5–5.0. Seismic stations used are shown as white squares in Fig. 1(a). A comparison of P-wave alignment for waveforms from KG2 station (Fig. 1a) using catalogue arrival times and cross-spectrum time differentials is shown in Fig. 3. In spite of large magnitude differences ranging from M1.5 to 5.0, we obtained precise alignment for the relocated earthquakes. Note that the location estimated from the correlation data is not the rupture initiation point (hypocentre) but instead corresponds to the centroid of the slip distribution, and the onsets of the first motion for the $M \sim 4.9$ earthquakes (No. 3, 32, 53, red colour in Fig. 3b) are not aligned with other smaller earthquakes. We used only the correlation data (i.e. the catalogue data were excluded) for the input of the double-difference relocation. The minimum number of correlation data per event pair is set to 30 to eliminate earthquakes whose locations are poorly constrained.

The centroids for 53 earthquakes before and after the relocation are shown in Fig. 4 and listed in Table 1. The number of earthquakes relocated is two times larger than in the previous study (Uchida *et al*. 2007). The relocation shows that earthquakes whose original hypocentres were distributed in a band 5 km long, 2 km wide and 6 km deep, running in the WNW–ESE direction, have centroids with separations of less than 2 km in any direction. The east–west cross-section (Fig. 4d) shows that the centroids have linear trend that probably delineates the surface of westward-dipping Pacific Plate. The estimated error in the relocation process is about 20 m, based on the residuals of the traveltime differentials. The results also indicate that there are several places where most of the earthquakes in the area are co-located. As shown in Fig. 5, we classified these small earthquakes into four groups based on the location of their centroids. Groups A and C are respectively located near the western and eastern edges of the source area of the $M \sim 4.9$ main shock. The size of the circles indicates the approximate size of the slip area assuming a stress drop of 38 MPa, which was estimated for the 2001 off-Kamaishi earthquake (Matsuzawa *et al*. 2001). Most of the

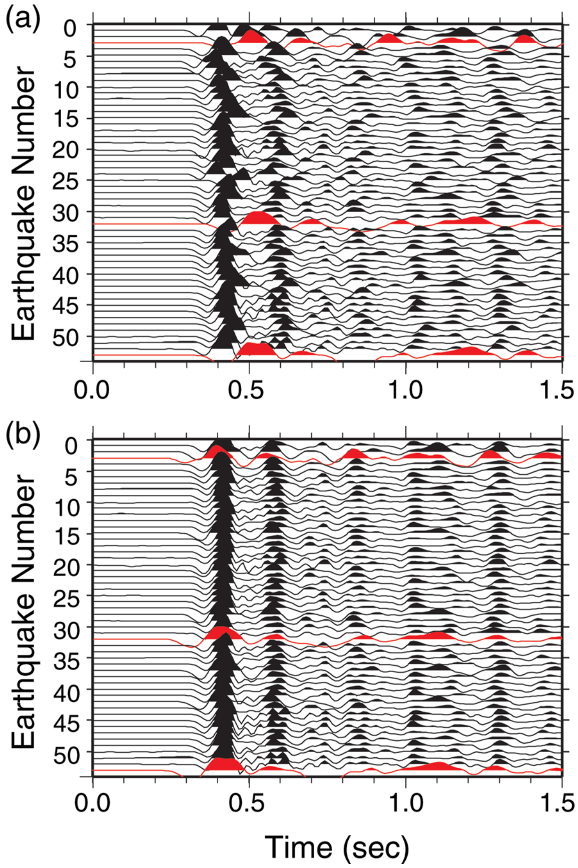

Figure 3. *P*-wave alignment for the 53 earthquakes used in this study recorded at KG2 station (Fig. 1a, $\Delta = 43$ km), in up–down component. (a) Alignment using catalogue arrival time. (b) Alignment using cross-spectrum time differentials. Waveforms are amplitude normalized and bandpass filtered between 1 and 10 Hz. The shading represents positive amplitude. Traces in red colour show 1995, 2001 and 2008 $M \sim 4.9$ events. Note that 21 earthquakes that could not directly estimated the differential time with the first earthquake (reference event) are also plotted based on differential traveltime with the earthquake that linked with the first event.

earthquakes in groups A and C seem to be co-located. Group B is located close to the centroids of the $M \sim 4.9$ earthquakes and some members appear to be co-located. Earthquakes in group D, which were not identified in the previous study (Uchida *et al*. 2007), are relatively small events (M1.6–1.9) located between groups B and C. The east–west cross-section (Fig. 5b) shows a clear alignment of these earthquake groups. A magnitude–time plot of these earthquakes together with other unrelocated earthquakes in the cluster (Fig. 2a) is shown in Fig. 5(c). Earthquakes in group A (red triangles) occur frequently and their activity is relatively stable in time. Earthquakes in group C (blue diamonds) also occur frequently, with a small gap (1–2 yr) just after the 1995 and 2001 $M \sim 4.9$ main shocks. Earthquakes in group B and D (green squares and pink hexagons), that seem to be located inside the slip areas for the $M \sim 4.9$ events, exhibit relatively large gaps (2–3 yr) after the 1995 and 2001 $M \sim 4.9$ main shocks.

4 SOURCE RADII, STRESS DROPS AND CUMULATIVE SLIPS

To understand the seismic process involved in an earthquake cycle, it is important to know source parameters, such as the source dimensions and the amount of slip. Following Imanishi & Ellsworth (2006) and Uchida *et al*. (2007), we calculated Fourier amplitude spectra for *P* and *S* waves using tapered 1.0 and 2.0 s time windows, respectively. The spectra were then resampled at equal log frequency intervals of $\Delta \log f = 0.025$, and smoothed using a running average of length $\Delta \log f = 0.2$. Spectral ratio for a pair of earthquakes recorded at the same station was calculated to eliminate site and path-dependent effects (Frankel & Wennerberg 1989).

For a robust measurement of the spectral ratios, we performed stacking of spectral ratios [multiwindow spectral ratio (MWSR) method of Imanishi & Ellsworth 2006)] We used three windows, overlapping by half of their duration, for three components at eight stations (black squares in Fig. 1a). These selected stations located 30–100 km from the earthquake cluster have good *S*/*N* ratios and available for almost the entire analysis period (1995–2008). All of the spectral ratios for the same event pair were stacked if they had a sufficient *S*/*N* ratio (>3). A maximum of 72 spectral ratios were stacked for a pair of earthquakes. A separate analysis was performed for *P* and *S* waves. Examples of stacked spectral ratios are shown in Fig. 6 (red bold lines) together with individual spectral ratios (black lines). The fluctuations in the spectral ratios have been successfully suppressed by the stacking procedure. For the 2001 and 2008 $M \sim 4.9$ main shocks, we observed some azimuthal variation in the pulse width of the first motion, probably suggesting directivity effect. However, the effect is weak for 1 sec three window stacked spectrum ratios. The corner frequencies for earthquake pairs appear to be consistent. For example, Figs 6(a)–(c) represent the spectral ratios of a M4.9 earthquake and an earthquake in group A, B and C, respectively.

Corner frequencies and seismic moments for 28 events of magnitude 2.4 or larger were estimated simultaneously using the multiple-empirical Green's function (MEGF) method (Ide *et al*. 2003), which is a slight modification of Hough (1997). Earthquakes of magnitude 2.4 or smaller were omitted from the analysis because they tend to have higher corner frequencies than the analysis limit (30 Hz), which is determined by the sampling frequency (100 Hz). We use the omega-square source model spectra proposed by Boatwright (1978) to model the stacked spectral ratio. We used a frequency band of 1–30 Hz (60 data points for each spectral ratio) for 383 and 377 event pairs (total numbers of equations were 22 980 and 22 620) for *P* and *S* waves, respectively. We used Levenberg–Marquardt algorithms for the iterative non-linear least-squares inversion. In the inversion, we set the seismic moment of the 2001 M4.8 event to be 1.12×10^{16} Nm, as estimated by Okada *et al*. (2003), because we needed one constraint to estimate the absolute scalar moments of each event. We then estimated the source radius (r) from the corner frequency (f_0) using the circular crack model of Sato & Hirasawa (1973),

$$r = \mathrm{C}v/2\pi f_0, \quad (1)$$

where v is the phase velocity (7.8 and 4.4 km s^{-1} for *P* and *S* waves, respectively) and C is a constant. We assumed C to be 1.5 for *P* waves and 1.9 for *S* waves.

The resulting source radii for the earthquakes are shown by circles in Fig. 7(a) and listed in Table 1. Although there is uncertainty derived from spectrum shape model, crack model and assumed phase velocity, the rupture dimension errors estimated from least-squares error of corner frequency are typically 6 per cent of their diameters. This small uncertainty comes from smooth stacked spectrum ratios and corner frequency consistency for all event pairs (single corner frequency for an earthquake well explain multiple spectrum

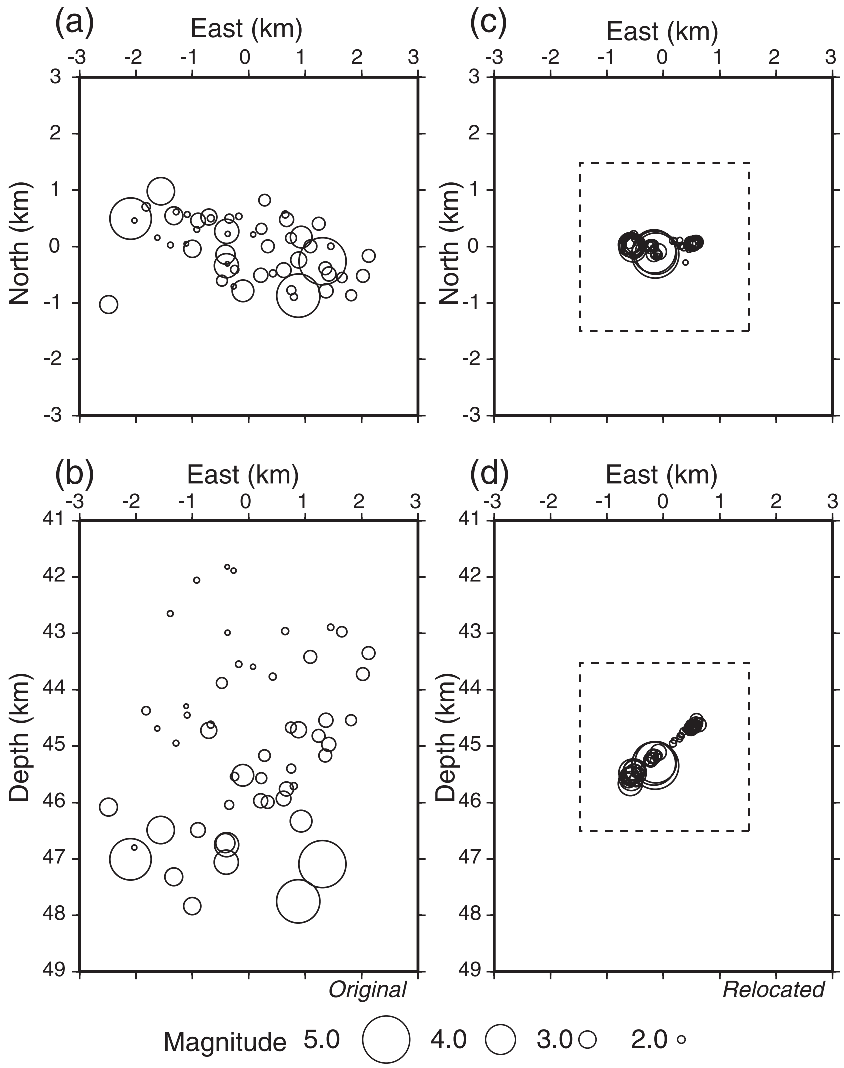

Figure 4. Hypocentre and centroid distribution of earthquakes in the off-Kamaishi cluster. (a) and (b) show original hypocentre locations and (c) and (d) show relocated centroid locations. Symbol size is proportional to magnitude and the scale is shown at the bottom of the figure. Dashed squares shown in Panels (c) and (d) are the areas shown in Figs 5(a) and (b), respectively.

ratios associated with other earthquakes). The centroids are projected onto a 38° westward-dipping plane based on the alignment of the centroids shown in Fig. 5(b). Although the slip areas of the earthquakes are likely more complex, we consider that circles centred on the centroids are a good first approximation. The source size of the 2008 $M4.7$ main shock (570 m) is very close to that of the 2001 $M4.8$ event (540 m), and most of the slip area is overlapping. Because we are plotting slip areas centred on its centroids, it will be hard to be not overlap the slip area for events with very close centroids. Earthquakes in groups A and C are located close to and about 100 m from the edge of the 2001 and 2008 $M \sim 4.9$ events, respectively. For small earthquakes the variability in earthquake slip is more important when discussing the overlap of source areas because the source location error is relatively large compared with the source dimensions. If two earthquakes are located in adjacent areas, the stress change due to one event will promote slip for adjacent area (promote successive occurrence of earthquake) whereas one location ruptured repeatedly, there will be no earthquake for a while due to stress release by the earthquake. There is one case that one earthquake occurred immediately after an earthquake in the group C (2 min in between), however most events occurred well separated in time (Fig. 5c). Therefore, most of the earthquakes in group A and C can also be assumed to be occurring repeatedly at the same location, considering the source sizes and location uncertainty. The earthquakes in group B, located near the centroids of the 2001 and 2008 $M \sim 4.9$ earthquakes, seem to be occurring at two adjacent locations. For earthquakes in group D, no source size was estimated because they are smaller than the magnitude threshold ($M2.5$) for the analysis. For a reference centroid of the latest earthquake in the group D is shown in Fig. 7(a).

Static stress drop ($\Delta\sigma$) was then calculated using the formula of Eshelby (1957):

$$\Delta\sigma = (7/16)(M_0/r^3), \tag{2}$$

where M_0 is seismic moment. As the final source radii and stress drops, we adopted the weighted averages of the values estimated from P and S waves, where the weights were set to be proportional to the number of spectral ratios in the stack.

The stress drops, indicated by colour in Fig. 7(a) and listed in Table 1, are higher for the 2001 $M4.8$ event (41 MPa) and the 2008 $M4.7$ event (27 MPa) than for other smaller earthquakes (3–11 MPa). Estimated errors in the stress drops are 6 and 2 MPa for the

Table 1. Estimated centroid locations, fault sizes and stress drops.

Group	Year	Mon.	Day	Hour	Min.	Sec.	Lat. (deg)	Lon. (deg)	Depth (km)	X (m)	Y (m)	Z (m)	X err (m)	Y err (m)	Z err (m)	M	f_c^P (Hz)	f_c^S (Hz)	r (m)	$\Delta\sigma$ (Mpa)	Mo (Nm)
C	1995	2	7	17	50	42.5	39.329150	142.103923	44.643	551.6	67.7	–436.8	11.5	8.0	14.0	2.6	–	–	–	–	–
A	1995	3	1	20	18	28.2	39.328254	142.091238	45.470	–542.2	–31.8	389.8	11.1	5.0	13.0	3.8	–	–	–	–	–
*M*5.0	1995	3	11	13	49	58.3	39.327249	142.095879	45.347	–142.0	–143.3	266.9	16.2	8.2	18.7	5.0	–	–	–	–	–
A	1995	9	25	0	12	50.3	39.328359	142.091458	45.452	–523.2	–20.1	371.8	10.0	4.5	10.5	3.4	6.6	5.8	256	5.7	2.05E+14
A	1997	1	28	8	1	56.6	39.328701	142.091652	45.422	–506.5	17.9	342.0	8.0	4.0	8.3	3.4	5.9	5.1	288	5.2	2.69E+14
C	1997	2	11	20	10	25.4	39.329036	142.104584	44.595	608.5	55.1	–484.6	8.9	5.2	9.9	2.3	–	–	–	–	–
C	1998	1	31	18	39	14.2	39.329260	142.104335	44.538	587.1	80.0	–542.3	7.4	4.3	8.2	2.6	13.8	10.8	129	5.3	2.55E+13
A	1998	4	26	9	50	26.9	39.329875	142.092422	45.436	–440.1	148.2	355.9	12.9	7.5	12.4	1.7	–	–	–	–	–
A	1998	4	30	0	23	45.0	39.328861	142.091483	45.462	–521.0	35.6	382.6	7.3	4.0	7.3	2.9	7.2	6.6	234	2.9	7.61E+13
B	1998	6	12	5	12	39.4	39.327070	142.096293	45.113	–106.3	–163.2	32.7	13.1	7.8	11.1	1.5	–	–	–	–	–
D	1998	6	15	4	46	42.6	39.328391	142.101664	44.739	356.8	–16.5	–340.5	9.6	5.8	8.1	1.9	–	–	–	–	–
C	1998	7	7	11	38	42.0	39.328442	142.102564	44.671	434.4	–10.9	–409.1	9.0	5.6	8.3	1.8	–	–	–	–	–
B	1998	9	2	8	58	29.4	39.327725	142.096506	45.112	–88.0	–90.5	32.2	8.0	4.7	6.3	2.9	10.3	8.2	172	4.9	5.54E+13
C	1998	10	16	21	22	17.0	39.329163	142.104267	44.597	581.2	69.2	–482.6	6.8	4.0	6.9	2.6	15.2	11.7	119	7.0	2.63E+13
A	1999	2	6	3	33	40.1	39.328472	142.091617	45.494	–509.5	–7.5	414.4	7.1	3.7	6.8	3.2	5.3	4.6	322	3.7	2.72E+14
B	1999	2	20	12	38	27.4	39.328707	142.095369	45.210	–186.0	18.5	130.5	7.5	4.5	7.1	2.4	13.7	10.8	130	3.1	1.54E+13
B	1999	3	5	10	51	31.0	39.328060	142.094066	45.288	–298.3	–53.3	208.2	12.5	7.5	10.8	1.6	–	–	–	–	–
C	1999	7	24	3	37	15.9	39.329289	142.104111	44.641	567.7	83.1	–438.9	7.0	4.0	7.3	2.6	13.2	10.6	133	4.1	2.14E+13
D	1999	11	6	17	48	1.2	39.328630	142.101090	44.821	307.3	9.9	–258.7	10.3	5.5	9.6	1.9	–	–	–	–	–
D	2000	4	30	1	12	39.2	39.325986	142.102058	44.707	390.8	–283.5	–373.1	14.3	8.0	13.5	1.6	–	–	–	–	–
A	2000	7	4	17	14	26.4	39.328879	142.091053	45.509	–558.2	37.6	429.2	8.1	4.5	8.0	3.1	7.4	6.8	223	5.2	1.20E+14
B	2000	8	3	16	8	19.2	39.328597	142.094880	45.255	–228.2	6.3	174.9	7.6	4.5	7.3	2.4	15.8	12.6	112	5.4	1.68E+13
C	2000	8	25	19	50	46.4	39.328922	142.103468	44.662	512.4	42.4	–418.2	6.5	3.8	6.8	2.7	16.3	12.4	111	11.1	3.45E+13
A	2001	7	20	0	39	39.9	39.329758	142.091575	45.493	–513.2	135.3	413.4	12.1	7.0	11.3	1.7	–	–	–	–	–
C	2001	8	15	5	56	46.4	39.328137	142.102774	44.684	452.5	–44.7	–395.7	7.6	4.4	7.2	1.9	–	–	–	–	–
C	2001	8	17	12	24	56.2	39.329009	142.103490	44.671	514.2	52.1	–408.4	6.5	3.8	6.5	2.7	14.8	11.6	120	8.2	3.22E+13
C	2001	8	17	12	27	28.2	39.328773	142.103999	44.634	558.1	25.9	–446.2	7.0	4.0	6.9	2.4	14.8	11	123	4.6	1.97E+13
A	2001	9	16	2	54	10.4	39.328784	142.090924	45.573	–569.3	27.1	493.3	7.1	3.8	7.1	3.6	5.2	4.3	331	4.9	3.97E+14
B	2001	10	3	21	10	54.2	39.328318	142.093514	45.325	–345.9	–24.6	245.5	9.1	5.4	7.9	1.5	–	–	–	–	–
B	2001	10	14	6	1	16.2	39.328525	142.094963	45.249	–221.0	–1.7	169.5	6.8	3.9	6.0	2.7	13.7	10.9	129	7.7	3.67E+13
B	2001	10	15	23	16	25.9	39.327077	142.095590	45.125	–167.0	–162.4	45.3	13.2	9.2	11.7	1.8	–	–	–	–	–
*M*4.8	2001	11	13	16	45	5.7	39.327775	142.095566	45.307	–169.0	–84.9	227.4	8.6	4.8	8.8	4.8	3	3.2	537	40.7	1.12E+16
C	2002	12	30	13	34	59.5	39.328691	142.103571	44.663	521.2	16.8	–417.3	7.2	4.3	7.1	2.2	–	–	–	–	–
A	2003	6	20	4	47	26.5	39.328855	142.090814	45.532	–578.7	35.0	452.6	9.0	5.2	8.3	3.0	10	8.8	169	6.3	6.51E+13
B	2003	9	21	19	54	22.9	39.326764	142.096019	45.180	–130.0	–197.2	100.5	11.0	7.3	10.1	1.6	–	–	–	–	–
C	2003	10	20	11	17	57.1	39.328765	142.103533	44.639	518.0	24.9	–441.3	8.5	5.1	8.5	2.6	14.7	11.3	122	5.2	2.14E+13
A	2004	7	18	4	22	1.6	39.328622	142.090669	45.532	–591.3	9.1	451.7	9.9	5.4	8.9	3.1	6.1	5.4	276	2.7	1.23E+14
C	2004	8	27	5	12	34.5	39.328943	142.103606	44.640	524.3	44.7	–439.6	9.4	5.1	9.2	2.6	14.4	10.4	128	4.8	2.31E+13
B	2004	8	30	11	40	5.5	39.327176	142.096414	45.169	–95.9	–151.4	89.1	10.6	6.8	10.1	2.1	–	–	–	–	–
B	2004	8	30	14	51	48.4	39.327313	142.095555	45.187	–169.9	–136.2	107.0	9.2	5.4	7.9	2.8	11	9	161	4.3	4.04E+13

Table 1. (*Continued*.)

Group	Year	Mon.	Day	Hour	Min.	Sec.	Lat. (deg)	Lon. (deg)	Depth (km)	X (m)	Y (m)	Z (m)	X err (m)	Y err (m)	Z err (m)	M	f_c^P (Hz)	f_c^S (Hz)	r (m)	$\Delta\sigma$ (Mpa)	Mo (Nm)
C	2005	6	3	23	9	39.0	39.329019	142.103067	44.681	477.8	53.2	–399.3	9.3	5.8	8.5	2.4	15.8	11.9	115	4.6	1.59E+13
A	2005	7	9	18	0	27.7	39.328817	142.090781	45.665	–581.6	30.8	585.5	8.4	4.8	8.5	3.6	4.8	4	361	4.7	4.93E+14
A	2005	7	9	22	37	5.0	39.330417	142.091409	45.587	–527.4	208.4	507.2	12.5	7.4	11.5	2.1	–	–	–	–	–
D	2005	9	11	19	35	52.6	39.329416	142.099555	44.952	175.0	97.2	–128.3	11.8	8.1	11.0	1.9	–	–	–	–	–
C	2006	1	5	12	12	16.8	39.329022	142.103238	44.688	492.5	53.5	–392.0	8.4	5.2	7.8	2.7	16	11.9	114	9.0	3.06E+13
D	2006	1	5	17	27	23.7	39.329540	142.100916	44.875	292.3	111.1	–204.7	12.9	9.3	14.5	1.7	–	–	–	–	–
B	2006	10	18	0	1	46.6	39.328553	142.094722	45.281	–241.8	1.4	201.0	9.3	5.9	7.8	2.2	–	–	–	–	–
A	2007	1	15	8	54	1.3	39.329402	142.090397	45.609	–614.7	95.7	528.9	9.5	5.2	8.4	2.8	9.7	8.6	172	5.6	6.06E+13
C	2007	2	25	17	24	55.1	39.329026	142.103016	44.703	473.4	54.0	–376.6	8.4	5.1	7.7	2.5	14.4	11.1	125	5.0	2.21E+13
B	2007	3	1	16	20	56.1	39.328357	142.095412	45.250	–182.3	–20.3	170.2	13.6	8.8	12.5	1.6	–	–	–	–	–
D	2007	10	8	8	36	46.7	39.328552	142.101239	44.807	320.2	1.3	–272.4	12.0	7.9	12.2	1.6	–	–	–	–	–
D	2008	1	9	10	41	18.5	39.329506	142.099774	44.904	193.8	107.2	–176.1	12.5	8.2	13.0	1.7	–	–		–	–
*M*4.7	2008	1	11	8	0	32.7	39.327410	142.095965	45.285	–134.6	–125.5	204.8	12.0	6.8	8.9	4.7	2.9	2.7	574	26.8	1.04E+16

X (eastward), Y (northward) and Z (depth) show the distance from the centroid of all the earthquakes. f_c^P and f_c^S are *P*- and *S*-wave corner frequencies, respectively. r is source radius and $\Delta\sigma$ is stress drop. Magnitudes were derived from JMA's catalogue.

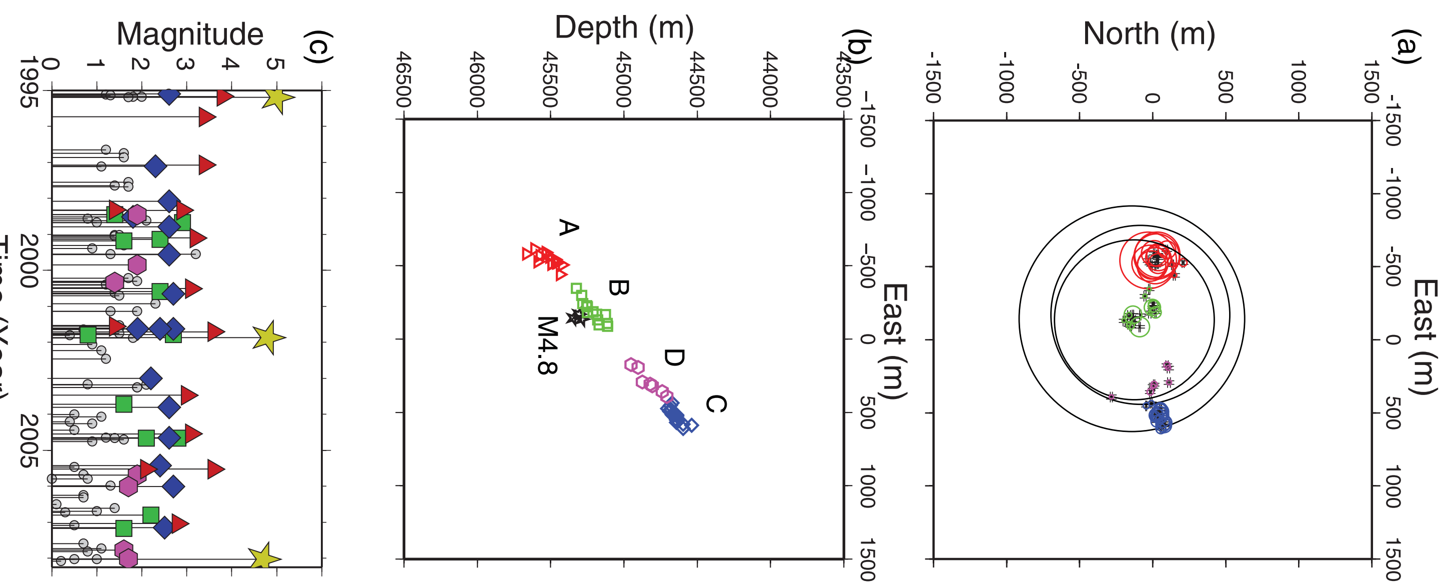

Figure 5. (a) Centroid distribution of earthquakes in map view. The approximate source size is indicated by the circle diameter and is calculated from seismic moment using the formula of Eshelby (1957), assuming a stress drop of 38 MPa (Matsuzawa *et al*. 2002). The seismic moment of each earthquake is calculated based on the relationship between seismic moment and magnitude (Hanks & Kanamori 1979). Horizontal errors are shown by black error bars. (b) East–west cross-section of the relocated centroids (circles). The circle size are the same for all earthquakes. The earthquakes in each subcluster (A–D) are indicated by a different colour. (c) Magnitude–time plot of off-Kamaishi earthquake cluster. Symbol colours as in Panels (a) and (b).

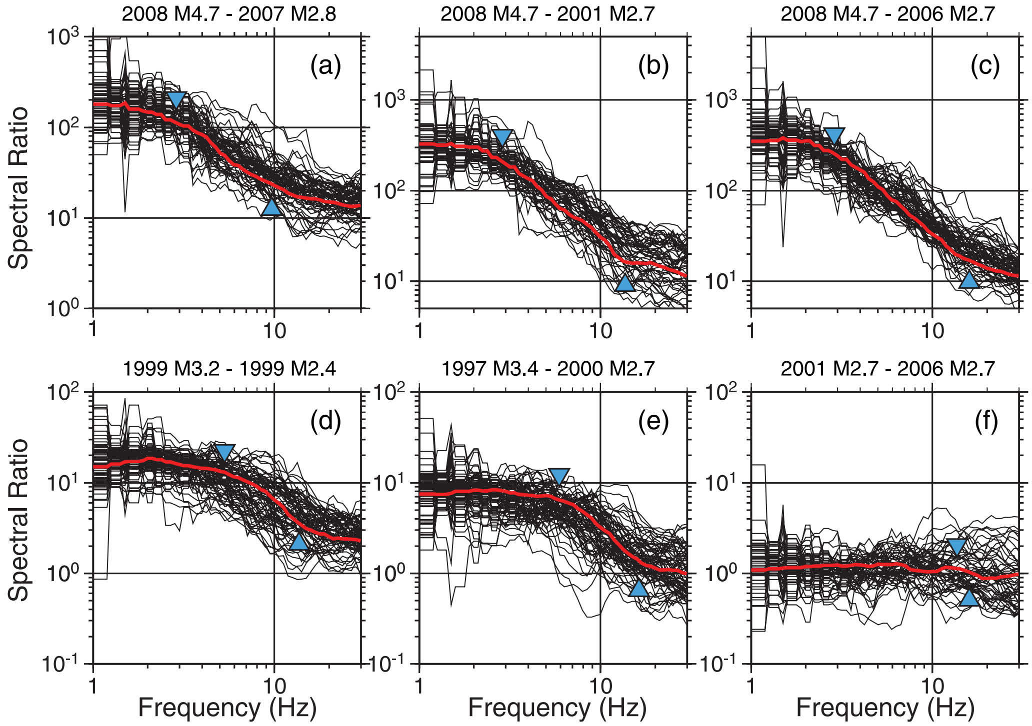

Figure 6. (a) Examples of spectral ratios for various time windows, components and stations (thin black lines) and stacked spectral ratio (red bold line). The event pairs are (a) 2008, $M4.7$–2007 $M2.8$ (group A), (b) 2008 $M4.7$–2001 $M2.7$ (group B), (c) 2008 $M4.7$–2006 $M2.7$ (group C), (d) 1999 $M3.2$ (group A)–1999 $M2.4$ (group B), (e) 1997 $M3.4$ (group A)–2000 $M2.7$ (group C), (f) 2001 $M2.7$ (group B)–2006 $M2.7$ (group C). Estimated corner frequencies (blue triangles) are also shown for each event estimated from the inversion of all stacked spectral ratios using an omega square model.

2001 and 2008 $M \sim 4.9$ events, respectively, and typically 0.7 MPa for the other smaller earthquakes.

The cumulative slips of groups A–C and $M \sim 4.9$ earthquakes are shown in Fig. 7(b). Here, the average slip for each earthquake is calculated from the seismic moment and source size assuming a rigidity of 4.0×10^{10} N m^{-2}. Group A has relatively constant slip and 21 cm slip in total. Groups B and C tend to have larger slip in the latter half of the cycle and the total slip are 6.3 and 15 cm, respectively.

5 SEISMICITY IN THE INTERSEISMIC PERIOD

Earthquakes in the cluster before 1995 were not relocated in this study due to an insufficient station coverage and a lack of timing accuracy. To investigate the spatio-temporal evolution of small earthquakes in the cluster over a longer period, we classified small earthquakes occurring before 1995 using a waveform similarity method. We first checked the coherence of waveforms among the earthquakes that were relocated in this study. We calculated the average and standard deviation of the coherence for a 40 s window in the 2–10 Hz frequency band at four stations that were in operation since 1985 (Table 2). We found that, within the same group, waveform coherence was large (0.82–0.94), whereas it was relatively small between groups (0.52–0.78). The coherences of intergroup pairs are usually outside of the standard deviation of the coherences between earthquakes in the same group (Table 2). This suggests that we can classify earthquakes into four the groups (A–D) using only the waveform similarity. Therefore, we classified the earthquakes from 1985 to 1995 using their average coherence with the earthquakes already identified. We assumed that an earthquake was a member of a certain group if the average coherence of its waveform with those of the group members was within one standard deviation of that for pairs within the same group. The results show that the tendency of earthquakes in groups B and D to occur late in the earthquake cycle applies also to the period before 1995 (Fig. 8a). About 77 per cent of earthquakes in group B and D occurred in the latter half of the earthquake cycles from 1985 to 2008. The grey triangles, stars and squares represent earthquakes outside the standard deviation but with an average coherence larger than 0.7 with the group. Although there may have been some erroneous assignments and failure of identifications due to incomplete waveform data, we succeeded in classifying the seismicity for four earthquake cycles. The absence of seismicity after $M \sim 4.9$ main shocks is prominent if we overlay all four earthquake cycles relative to the occurrence times of the main shocks (Fig. 8b). The overlaid plot for 2 hr before and after the $M \sim 4.9$ earthquakes (Fig. 8c) shows that there are several aftershocks immediately following the $M \sim 4.9$ earthquakes. However, we could not estimate their precise location because they are too small to obtain enough differential times by cross-spectrum method.

6 RUPTURE INITIATION POINTS FOR THE $M \sim 4.9$ EVENTS

Rupture initiation points are an important information on earthquake characteristics and the behaviour of the asperity in the final stage of the earthquake cycle. As described in Section 3, we obtained the precise locations of the earthquake centroids using a waveform correlation approach. However, we do not know the precise locations of the rupture initiation points (hypocentres). This information cannot be obtained using the same waveform correlation technique

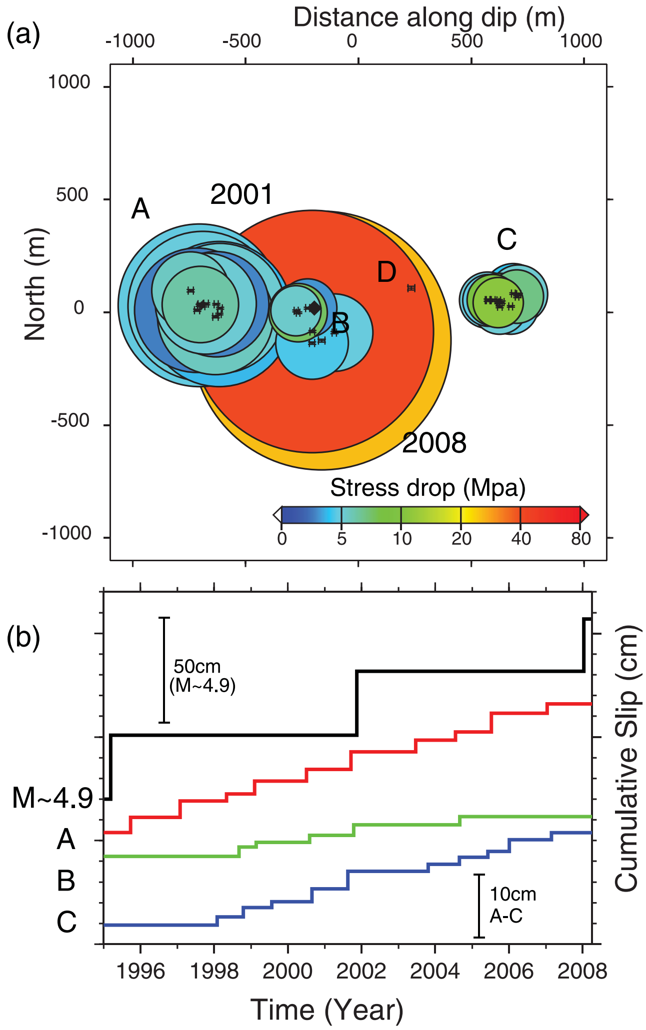

Figure 7. (a) Location, rupture area and static stress drop for the earthquake cluster projected on a 38° westward-dipping plane. Circles denote source sizes and their centres represent the earthquake centroids. Small bars denote 2σ centroid location errors. Colour indicates stress drop. (b) Cumulative slip of repeating earthquakes for $M \sim 4.9$ sequence, group A, group B and group C. The slip amount for the 1995 M5.0 earthquake was assumed to be the same for the 2001 earthquake (31 cm) because we do not have slip estimation for this earthquake. Note that the vertical scale are different for the $M \sim 4.9$ sequence and groups A–C.

Table 2. Averaged coherence of waveforms for the earthquakes between and within groups. Value in parentheses show standard deviation.

	A	B	C	D
A	0.82 (0.11)	0.52 (0.22)	0.53 (0.19)	0.60 (0.14)
B	0.52 (0.22)	0.86 (0.06)	0.60 (0.19)	0.78 (0.13)
C	0.53 (0.19)	0.60 (0.19)	0.94 (0.09)	0.77 (0.07)
D	0.60 (0.14)	0.78 (0.13)	0.77 (0.07)	0.88 (0.12)

because the hypocentres should be estimated from arrival times of initial motions of P and S waves and it is difficult to obtain cross-spectrum time differentials. To obtain accurate timing of the initial motions from seismograms, we used the method of Shimamura *et al.* (2011) that utilizes the ratio of the double difference of the P- and S-wave arrival times,

$$\left(t^1_{S,a} - t^1_{S,b}\right) - \left(t^2_{S,a} - t^2_{S,b}\right) = \gamma\left[\left(t^1_{P,a} - t^1_{P,b}\right) - \left(t^2_{P,a} - t^2_{P,b}\right)\right], \tag{3}$$

where t_P and t_S are the arrival times of P and S waves, respectively, γ is the V_P/V_S ratio, the superscripts 1 and 2 indicate earthquakes and the subscripts a and b indicate stations. This equation was derived from the relationship between the ratio of the traveltime of P and S waves (Shimamura *et al.* 2011). For earthquake 1 and stations a and b, the S-wave traveltime is related to the P-wave traveltime using γ as,

$$t^1_{S,a} - t^1_O = \gamma\left(t^1_{P,a} - t^1_O\right), \tag{4}$$

$$t^1_{S,b} - t^1_O = \gamma\left(t^1_{P,b} - t^1_O\right), \tag{5}$$

where ${t_O}^1$ is the origin time of earthquake 1. Subtracting eq. (5) from eq. (4), we obtain,

$$t^1_{S,a} - t^1_{S,b} = \gamma\left(t^1_{P,a} - t^1_{P,b}\right). \tag{6}$$

A similar equation can be obtained for earthquake 2 and by subtracting it from eq. (6), we obtain eq. (3).

This equation shows that the double difference of the arrival time must be located on a line with a slope corresponding to the V_P/V_S ratio. We utilized this idea to check the outliers of the phase readings. We plotted the double differences, that is, $(t^1_{S,a} - t^1_{S,b}) - (t^2_{S,a} - t^2_{S,b})$ and $(t^1_{P,a} - t^1_{P,b}) - (t^2_{P,a} - t^2_{P,b})$, for all earthquake pairs in one figure. We selected outliers (points far from the best fit line) and re-read or discarded the phase readings depending on the quality of the waveform. Fig. 9 shows examples of P- and S-wave first motions. The timing errors for first arrivals are about 0.01 and 0.05 s for P and S waves, respectively. We carefully choose the first motions of the 2001 and 2009 $M \sim 4.9$ earthquakes in addition to nine $M > 2.0$ earthquakes in the cluster since 2005 that are clearly recorded at many stations. We used eight stations that are located within 70 km of the epicentres of the earthquakes. Examples of the original and refined S picks are also shown in Fig. 9(b). For the P picks, the original and refined one are the same for the 2008 earthquake. The final and original double-difference plot of the data is shown in Fig. 10. The original arrival data show scattered S double difference (Fig. 10a) whereas final double-difference data are located within about 0.05 s from the best-fit line. Most of improvement comes from S pick of the nine small earthquakes. Here, we assumed V_P/V_S ratio of 1.73, which is consistent with local seismic tomography analyses in this region (e.g. Tsuji *et al.* 2008).

To estimate the relative locations of the hypocentres of the $M \sim 4.9$ earthquakes with respect to their centroids, we use the centroids of the nine small earthquakes as references. We fixed (constrained) the hypocentres of small earthquakes to their centroids in the iteration procedure of the double-difference relocation method and estimated the hypocentres of the 2001 and 2008 $M \sim 4.9$ main shocks. This method takes advantage of precise relative centroid location among the reference earthquakes and the $M \sim 4.9$ events (Section 3) and relatively small separation between centroids and hypocentres for the small reference earthquakes. The separation (distance) between centriod and hypocentre of the reference earthquakes are less than 360 m because the estimated source sizes are less than the size (Section 4). We ignored the error associated with the hypocentre-centroids separation to estimate the rough locations of the hypocentres within the rupture area (~1 km in diameter).

Both $M \sim 4.9$ hypocentres were located in the southeastern part of the source area (Fig. 11). This is the shallow side of the asperity and is not the site of the small earthquakes (groups A–D) that occur

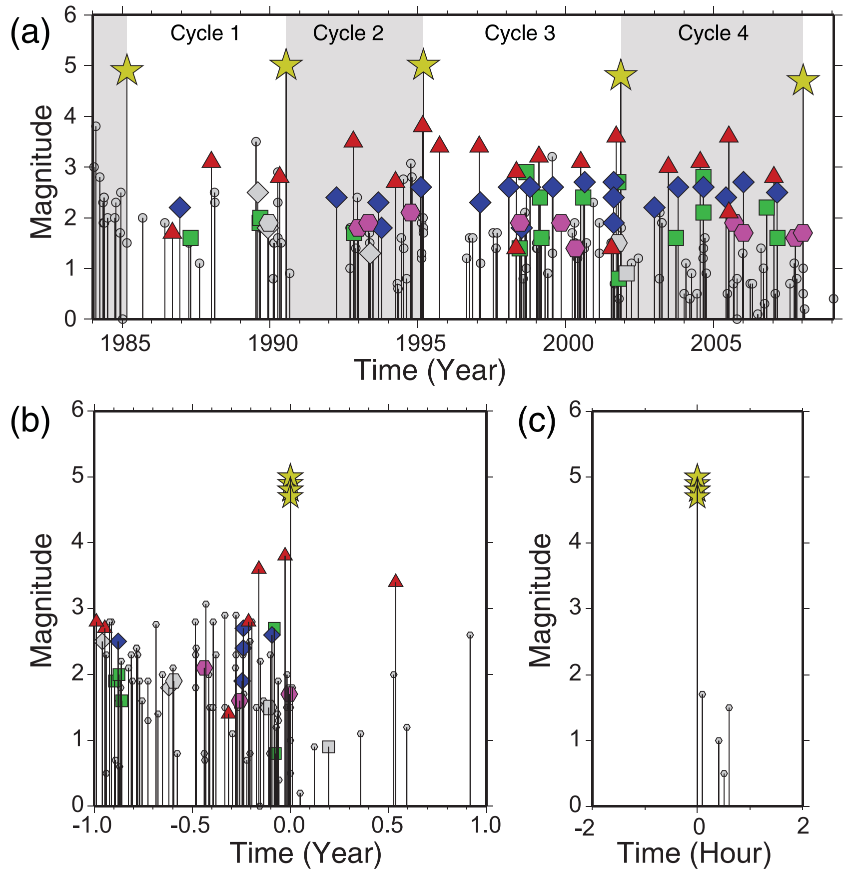

Figure 8. (a) Magnitude–time plot of off-Kamaishi earthquake cluster for the period from 1984 to 2009 January 25. Yellow stars, red triangles, green squares, blue diamonds and pink hexagons denote $M \sim 4.9$ sequence, group A, group B, group C and group D, respectively. The grey triangles, squares, diamonds and hexagons are earthquakes that are classified to group A, group B, group C and group D without enough confidence (see main text for detail). Shaded and unshaded area show four earthquake cycles (cycles 1–4). (b) Magnitude–time plot for one year before and after the $M \sim 4.9$ sequence. The data for 1985, 1990, 1995, 2001 and 2008 earthquakes are collapsed based on the occurrence time of the each earthquake. (c) The same as Panel (b) but for 2 hr before and after the $M \sim 4.9$ sequences. The symbols in Panels (b) and (c) are the same as that in Panel (a).

during the interseismic period. The relocation results obtained without fixing the locations of the small earthquakes (Figs 11c and d) confirm this result because the relative locations of the hypocentres are similar to the final results (Figs 11a and b). Note that we do not have the location of the $M \sim 4.9$ centroid in Figs 11(c) and (d) because there is no data to relate hypocentre and centroid in this simple hypocentre location. Estimations using a bootstrap method (Figs 11a and b) give a location error of about 500 m. Okada *et al* (2003) and Shimamura *et al*. (2011) also estimated slip distributions for the 2001 and 2008 $M \sim 4.9$ earthquakes relative to their hypocentres from seimic waveform inversion. Both results show the hypocentres are located to the east of the centroid, consistent with our result, but closer to the centroids (centre of the slip area). Our results rather indicate that the hypocentres are located near the SE edge of the slip area, although the error ellipsoid is elongated in the SE–NW direction close to the centroids of the $M \sim 4.9$ main shocks. Therefore, we investigated whether the hypocentres could be located near the centroids of the $M \sim 4.9$ events (NW edge of the error ellipsoid). For this purpose, we estimated the theoretical arrival time of P wave if the hypocentre is located near the centroid. The estimation was performed by assuming zero differential traveltime with an earthquake located at group B that is located near the centroids of the $M \sim 4.9$ earthquakes. Although we have ambiguity in absolute arrival time, the estimated theoretical arrival time (white triangles in Fig. 9a) clearly does not coincide with the observed P-wave first motion (black triangles in Fig. 9a). This means the hypocentre is not located near the centroids of the $M \sim 4.9$ main shocks but are instead located near their SE edges.

7 DISCUSSION

7.1 Earthquake cycle and seismicity in the interseismic period

The recurrence of earthquakes and the nature of earthquake cycles are fundamental problems in seismology. Numerical simulations using the laboratory-derived laws of friction are useful for studying earthquake cycles (e.g. Yoshida & Kato 2003; Kato 2004; Ariyoshi *et al*. 2007; Chen & Lapusta 2009). Precise observational data in the earthquake cycle are needed to validate the predicted behaviour of recurrent earthquakes and to assimilate the observations. However, it is not easy to carry out precise, stable and long-term observations over multiple earthquake cycles. Small repeating earthquakes occur frequently and are analysed to study earthquake cycles (e.g. Nadeau *et al*. 2004; Chen *et al*. 2010). However, these analyses mainly concentrate on the main sequence and the process during the whole earthquake cycle is not well known. The $M \sim 4.9$ off-Kamaishi repeating earthquakes are relatively large and provide a unique

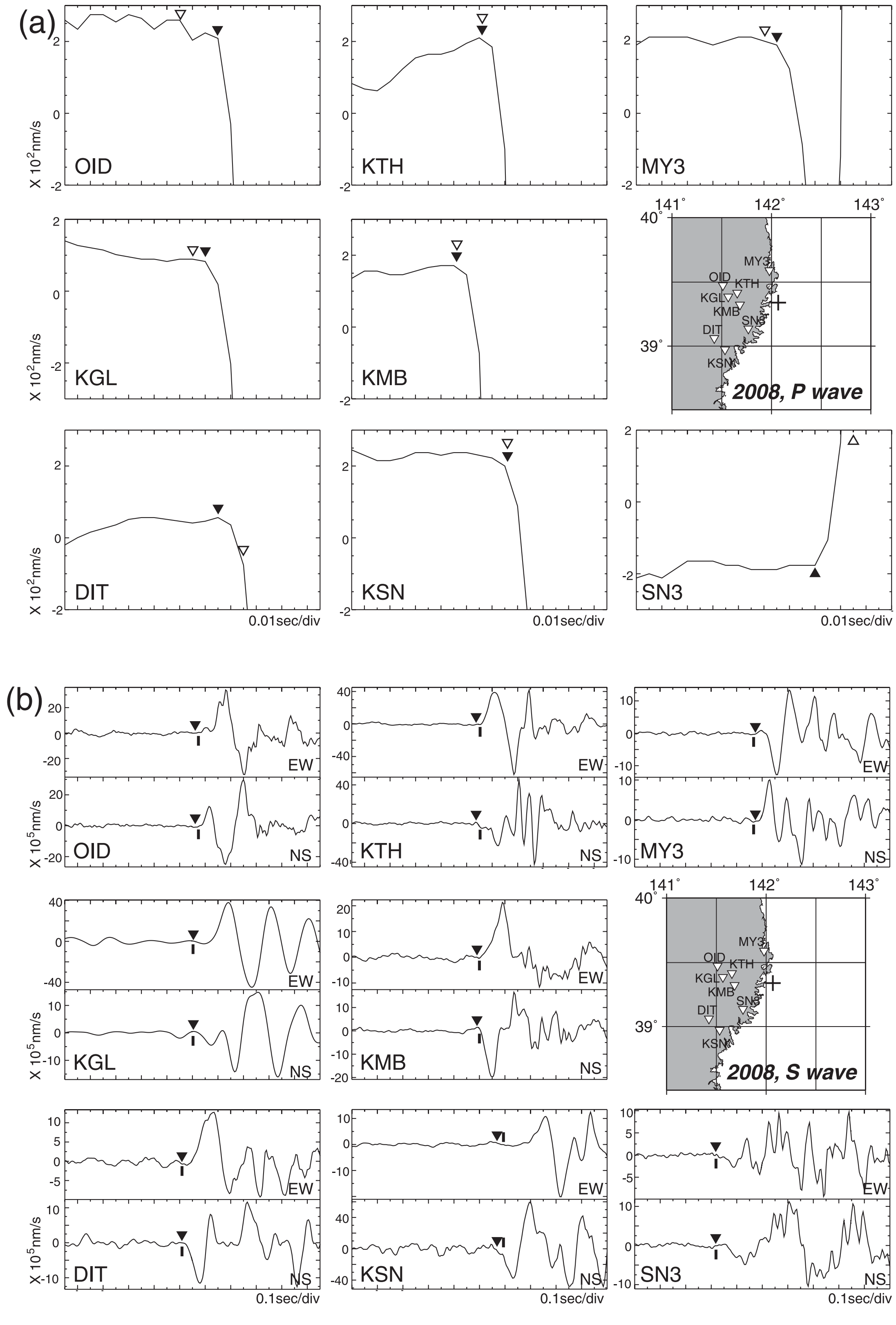

Figure 9. (a) *P*- and (b) *S*- velocity seismogram around the first motion for the 2008 $M \sim 4.9$ earthquake recorded eight stations used in this study. Black triangles show chosen locations of first motions. White triangles in Panel (a) show theoretical arrival time of *P* wave to position the hypocentre of the earthquake at its centroid. Right middle map shows the location of the stations (white reverse triangles) and of the $M \sim 4.9$ earthquake (cross). The full scale of each trace is 500 nm s^{-1} for Panel (a) and the maximum amplitude in the window for Panel (b). Black bars in Panel (b) show original *S* pick before the refinement of picks by the procedure described in Section 6.

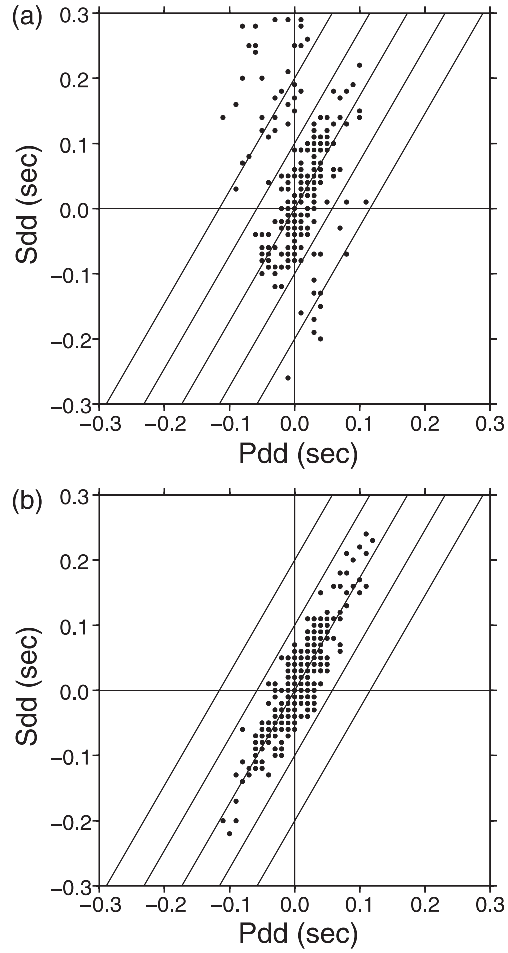

Figure 10. Relationship between double difference of *P* (*P*dd) and *S* wave (*S*dd). Panel (a) shows original double difference and Panel (b) shows refined double difference. One of the two stations was fixed to the KGL station as a reference and all available event pairs are plotted here. Thin straight lines show ideal lines corresponding to γ (Vp/Vs) = 1.73.

opportunity to observe not only the recurrence of main shocks but also to infer the process occurring in the interseismic period from the activity of the small accompanying earthquakes at the asperity.

The relocation results for the earthquake cluster suggest that the three recent main shocks (1995, 2001 and 2008 earthquakes) are co-located with each other (Fig. 5a). Most of the small earthquakes in the interseismic period occur inside or near the edge of the slip area of the mainshock sequence (Fig. 7a). Slip distribution for the earthquake cycle before the 2001 main shock and that before the 2008 main shock are shown in Fig. 12(a) and (b), respectively. Average slip values are calculated from the seismic moment and source size assuming a rigidity of 4.0×10^{10} N m^{-2}. Interestingly, the amount of slip near the edge of the mainshock slip area is relatively large during an earthquake cycle. The amounts of slip in the interseismic period for groups A and C are comparable and are about 25–40 per cent of the coseismic slip of the $M \sim 4.9$ main shocks. This probably corresponds to repeated slip due to the concentration of stress in the main asperity by aseismic slip in regions surrounding it (i.e. stress concentration between locked and creeping areas). Similar small repeating earthquake activity is seen along the San Andreas fault as 'streaks' (Waldhauser *et al*. 2004). The slip amount near the centre of the main asperity was about 5–15 per cent of the coseismic slip of the $M \sim 4.9$ events. The fact that the slip distributions for both cycles are similar suggests that not only the main shocks but also the process occurring during the earthquake cycle are similar. These results suggest the possibility of monitoring the interseismic process through observations of small earthquakes in and around the asperity of the main shock for the case of simple and independent system.

The slip amount estimated in this study is average slip on circular area (the peak slip amount can be larger than the estimated slip amount). Therefore, we try to estimate the averaged seismic coupling on the slip area for the $M \sim 4.9$ earthquakes. We compared the averaged slip with the slip deficit for each cycle assuming the slip deficit rate of 8.3 cm yr^{-1} (dashed line in Fig. 12) and 4.5 cm yr^{-1} (dotted line in Fig. 12). The former one is taken from the plate convergence rate (DeMets *et al*. 1994) because the region surrounding the asperity for the Kamaishi–Oki earthquake is thought to be decoupled (Matsuzawa *et al*. 2002; Uchida *et al*. 2005). The latter one is calculated from interplate coupling rate that is estimated form the GPS data in 1997–2001 around the off Kmaishi region (Suwa *et al*. 2006). The coseismic slips for the 2001 and 2008 $M \sim 4.9$ earthquakes (31 and 25 cm, respectively) are smaller than the accumulated slip deficits (55 and 51 cm, respectively) in the two interseismic periods expected from the plate convergence rate (8.3 cm yr). For the case of 4.5 cm yr^{-1} slip deficit rate, the coseismic slips for the 2001 and 2008 $M \sim 4.9$ main shocks are comparable with the accumulated slip deficit (30 and 28 cm, respectively). In this case the coupling coefficient on the slip area for the $M \sim 4.9$ earthquakes is close to 100 per cent. We need more precise slip distribution and slip deficit estimates to discuss the absolute value of coupling of the $M \sim 4.9$ asperity.

7.2 Slip inside the asperity

Numerical simulations using laboratory-derived laws of friction show occurrence of aseismic slip in the coseismic slip area preceding recurrent earthquakes (e.g. Yoshida & Kato 2003; Kato 2004; Ariyoshi *et al*. 2007; Chen & Lapusta 2009; Hori & Miyazaki 2010). A large preseismic slip near the edge of the coseismic slip area and aseismic slip migration to the centre of the coseismic slip area are sometimes seen in these numerical simulations (Yoshida & Kato 2003; Kato 2004; Ariyoshi *et al*. 2007; Chen & Lapusta 2009; Hori & Miyazaki 2010). Chen *et al*. 2010 discussed the recurrence interval and seismic moment variation for small repeating earthquake at Parkfield based on earthquake simulations. They found that the seismic moment variation depends largely on the critical slip distance and asperity size, and aseismic slip plays an important role. The slip for group B, which is close to the centre of the coseismic slip area for the main shock, probably represents aseismic slip migration into this area (unfastening of the asperity), as discussed in Uchida *et al*. (2007). This idea is proposed because loading by aseismic slip in the interseismic period near group B is necessary to rupture the asperity of the group B events. In this study, we found another earthquake cluster (group) located in the coseismic slip area of the main shocks (group D, Fig. 5) and it is also associated with aseismic slip during the interseismic period. The earthquake cycle simulations performed by Yoshida & Kato (2003) showed a very similar unfastening of the asperity during the interseismic period. Recently, Hori & Miyazaki (2010) simulated the occurrence of earthquakes inside an asperity to model the seismicity of the off-Kamaishi earthquake cluster. Their hierarchical asperity model successfully reproduces the observed earthquake activity.

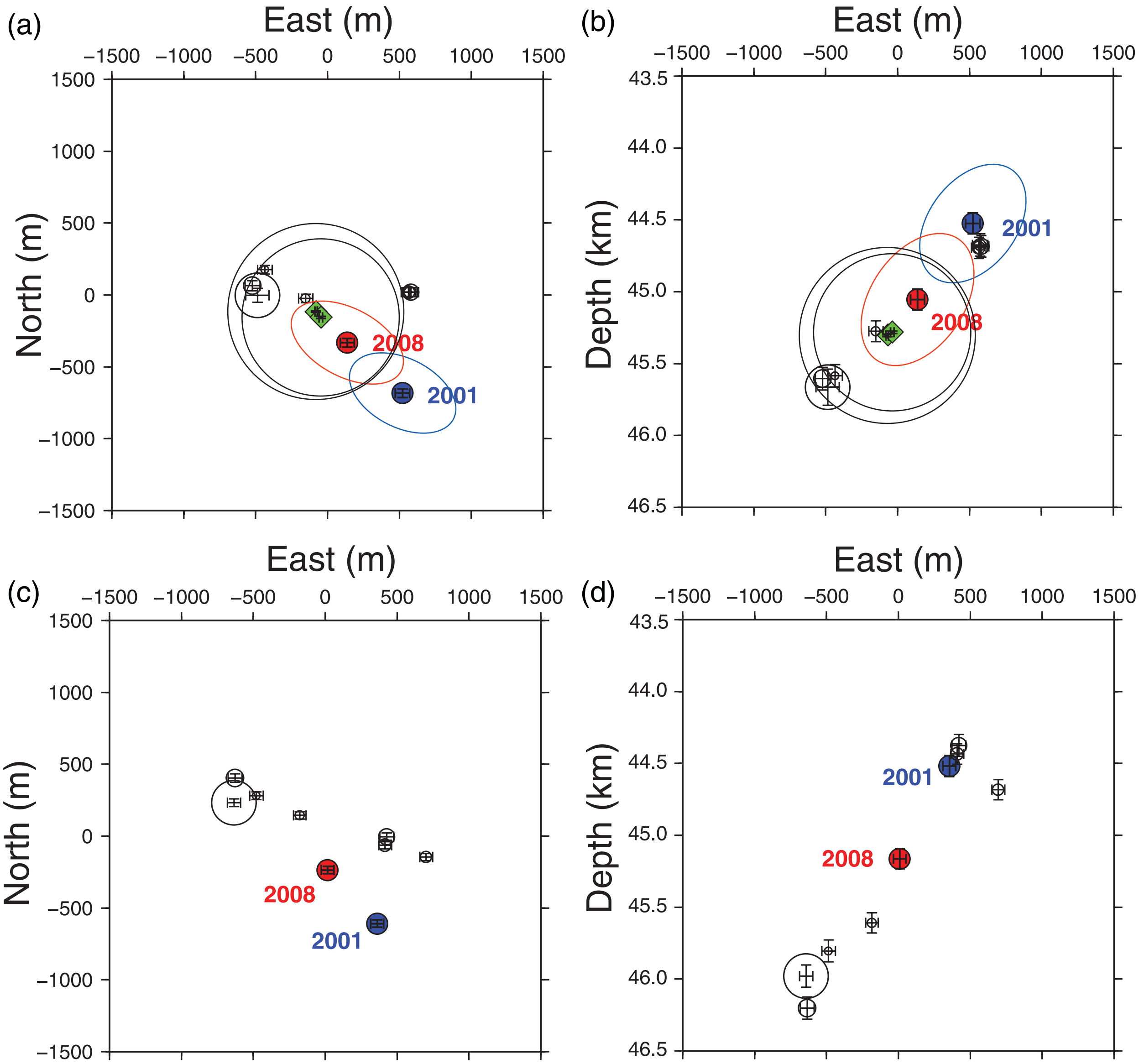

Figure 11. (a) and (b): Locations of hypocentres for the 2001 and 2008 $M \sim 4.9$ earthquakes relative to their centroids and other nine small earthquakes in the off-Kamaishi earthquake cluster that are used as references. (a) Shows map view and (b) shows east–west cross-section. Approximate source size is indicated by circle diameter and is calculated using the formula of Eshelby (1957), assuming the stress drops of the earthquakes are 38 MPa. The black error bars show the centroids of each earthquake. Filled circles and ellipsoids indicate the location of hypocentres (initial break points) and uncertainty for the 2001 (blue) and 2008 (red) $M \sim 4.9$ earthquakes. Green diamonds show centroids for the 2001 and 2008 $M \sim 4.9$ earthquakes (c) and (d): Location of hypocentres for the 2001 and 2008 $M \sim 4.9$ and nine small earthquakes in the off-Kamaishi earthquake cluster. No constraints on centroid location are applied for this relocation.

7.3 Episodic intrusion of aseismic slip?

To investigate the spatio-temporal evolution of small-earthquake activity in the off-Kamaishi earthquake cluster, we plotted the location of the earthquake along the dip versus the timing of earthquake (Fig. 13a). In almost all cases, earthquakes in group A are seen to precede those in group B, with the time interval being within 2 months in most cases. On the other hand, we could not find any clear relationship between groups C and D and $M \sim 4.9$ earthquakes and other groups (A–D). For nine successive earthquakes in groups A and B that occurred within 50 days (red and green filled symbols), we plotted the relationship between the time elapsed because the group-A earthquake and the distance between the tip of the group-A earthquake and the centroid for the group-B earthquake (Fig. 13b). The results indicate a proportional relationship between distance and time interval. This probably represents triggering of group-B earthquakes due to propagating aseismic slip (after slip) from group-A earthquake location. Because group A is located near the western tip of the asperity for the $M \sim 4.9$ main shocks and group B is located close to the centroid of the main shocks, this may indicate episodic occurrence of aseismic slip at deeper parts of the asperity and its upward migration towards the mainshock centroid, triggering group-B earthquakes.

In Fig. 13(b), all of the data points are below the 9 m day^{-1} line. If this represents the migration speed of aseismic slip in the asperity, it is smaller than the tremor migration speed at the Nankai trough (8–420 m hr^{-1}; Ueno *et al*. 2010), Cascadia (5–10 km day^{-1}; Kao *et al*. 2006) and San Andreas fault (15–40 km hr^{-1}; Shelley *et al.* 2009). These tremors are located outside the coseismic slip areas for large earthquakes whereas the successive earthquakes in the

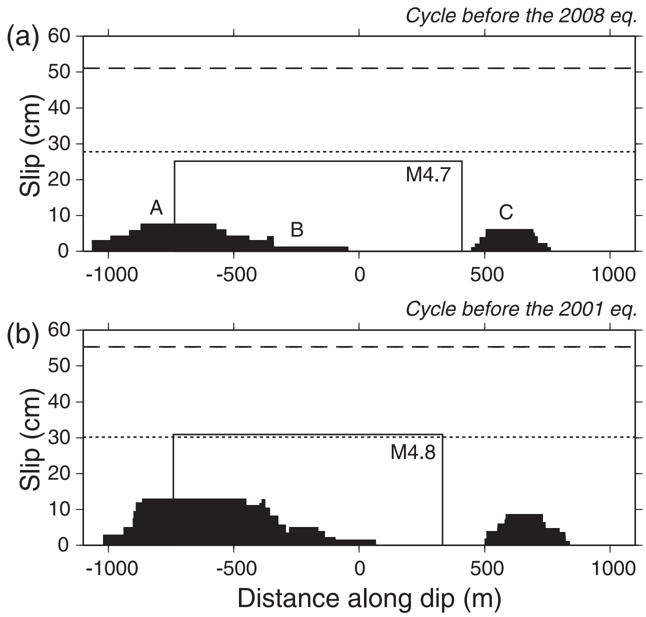

Figure 12. Cumulative slip of earthquakes in the interseismic period of the earthquake cycle (a) before the 2008 $M4.7$ earthquake (time period from just after the 2001 earthquake to just after the 2008 earthquake) and (b) before the 2001 $M4.8$ earthquake (time period from just after the 1995 earthquake to just after the 2001 earthquake). The slip area and amounts of the 2001 and 2008 earthquakes are also shown in white rectangles. The slip amounts are calculated from the seismic moment and source size estimated in this study by assuming a rigidity of 4.0×10^{10} N m^{-2}. Dashed and dotted lines denote slip deficit in the interseismic period assuming 8.5 cm yr^{-1} and 4.5 cm yr^{-1} slip deficit, respectively.

off-Kamaishi region are located inside the coseismic slip areas for the $M \sim 4.9$ earthquakes. This difference in migration speed might be due to the slip properties of the faults. Other possibility of the triggering mechanism is pore-pressure diffusion because water is one of an important mechanism to produce subduction zone earthquake. Seismicity migration speed of ~15m day^{-1} was observed for reservoir induced seismicity and explained by pore-pressure diffusion within a heterogeneous fault zone (El Hariri *et al*. 2010). This migration speed is comparable to our observation.

7.4 Characteristics of mainshock sequence

The rupture initiation points (hypocentres) are located near the southeastern edge of the asperity (Fig. 11). One possible explanation for this is that the slip area of the off-Kamaishi $M \sim 4.9$ main shocks consists of several asperities, the main (and strongest) one containing the hypocentres of the $M \sim 4.9$ earthquakes and the others corresponding to groups A–D. These asperities may rupture simultaneously and give rise to slip in the entire region. If there exists a large difference in strength between the main and secondary asperities, earthquakes of the secondary asperities corresponding to the in groups A–D do not trigger slip of the entire region. Other possibility is that a local aseismic slip fluctuation (acceleration) close to the hypocentres induces the occurrence (start of rupture) of the $M \sim 4.9$ main shocks. The Kamaishi–oki sequence is located near the depth limit for interplate earthquakes (Igarashi *et al*. 2001) and the area further deep is thought to be stably sliding. Thus, a fluctuation in aseismic slip would most likely originate from the shallower portion due to the occurrence of afterslip, as discussed in Uchida *et al*. (2005). However, at present we do not have any

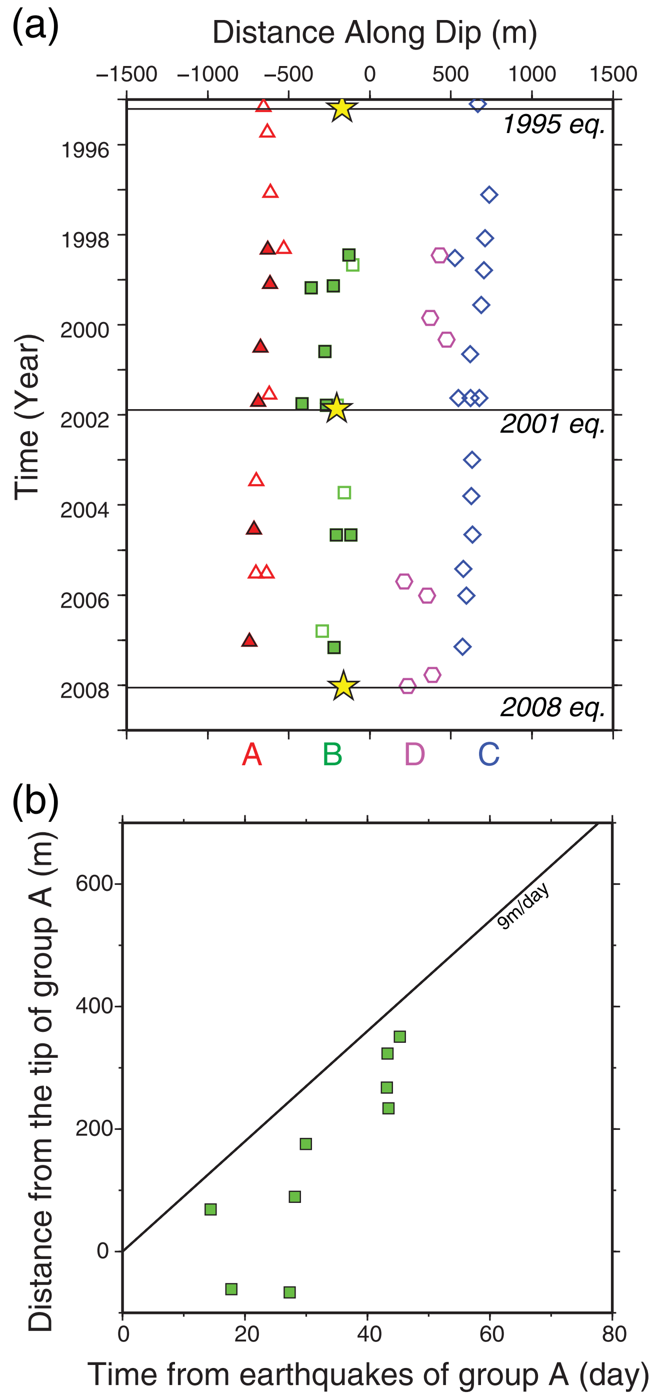

Figure 13. (a) Spatio-temporal plot of 53 relocated earthquakes in the off-Kamaishi cluster from 1995 to 2008 (the same earthquakes plotted on Figs 5a and b). Horizontal axis shows distance along dip of the earthquake alignment (along 38° westward-dipping fault plane, plus sign indicates east). Red triangles, green squares, pink hexagons and blue diamonds show earthquakes classified as group A, B, D and C, respectively. Stars and horizontal bars show the location and timing of $M \sim 4.9$ earthquakes. Filled red triangles and green squares show earthquakes that occurred within 50 days in groups A and B. (b) Spatio-temporal relationship between earthquakes in group B and group A. Horizontal axis shows the delay between group-B and group-A earthquakes. Vertical axis shows distance between the centroids of group B and the tip of the source area of earthquakes in group A. The source area of earthquakes in group A was taken from the radius of the slip area estimated in Section 4.

evidence for such fluctuation before the 2001 and 2008 earthquakes. The rupture initiation points are most likely determined by strength heterogeneity because the $M \sim 4.9$ earthquakes give rise to higher stress drops that are probably attributed to strong asperities.

8 CONCLUSIONS

We have estimated the parameters for $M \sim 4.9$ main shocks and their accompanying microearthquakes over two earthquake cycles in the Kamaishi–oki sequence. The $M \sim 4.9$ sequence ruptures at almost the same location, and the source parameters, including the hypocentres for the 2001 and 2008 earthquakes, were similar to each other. Microearthquakes in the interseismic period were also found to have occurred in basically the same manner over four earthquake cycles. Earthquakes in clusters near the deeper and shallower edge of the $M \sim 4.9$ asperity occurred repeatedly at the same location and the cumulative slip was about 25–40 per cent of the coseismic slip of the $M \sim 4.9$ earthquakes. We also found relatively inactive earthquake clusters in the coseismic slip areas for the $M \sim 4.9$ main shocks. Slip amount by these clusters was about 5–15 per cent of the coseismic slip of the $M \sim 4.9$ main shocks. This difference of interseismic slip probably indicates that co-seismic slip near the centre of the slip areas is large compared to that near the edge. Earthquake clusters near the mainshock centroids become active during the period before the $M \sim 4.9$ main shocks, which probably represents unfastening of the asperity. The successive occurrence of earthquakes in groups near the edge and centre of the mainshock asperity is probably an indication of the periodic intrusion of aseismic slip. The final rupture of the $M \sim 4.9$ earthquakes for 2001 and 2008 is estimated to have started at the southeast part of the asperity and the stress drops of these earthquakes are higher than those of the others. Our tentative explanation is that a strong asperity near the hypocentres of the main shocks governs the occurrence of the main shocks, and the small earthquakes during the interseismic period are an indication of aseismic slip intrusion to the mainshock asperity. If this kind of unfastening and seismicity occur in other interplate earthquakes, it is expected to be a good estimator of the state of the asperity.

ACKNOWLEDGMENTS

We thank T. Nakayama at Tohoku University for his cooperation in editing the waveform data, J. Rubinstein and M. Matsubara at U.S. Geological Survey for thoughtful comments on this manuscript. This work was supported in part by the Global COE Programme, ‘Global Education and Research Center for Earth and Planetary Dynamics’ at Tohoku University. The authors thank R. E. Abercrombie, anonymous reviewer and editor E. Fukuyama for their thoughtful reviews of the manuscript. Some of the figures were drawn using Generic Mapping Tools software (Wessel & Smith 1995).

REFERENCES

Ariyoshi, K., Matsuzawa, T., Hino, R. & Hasegawa, A., 2007. Triggered non-similar slip events on repeating earthquake asperities: results from 3D numerical simulations based on a friction law, *Geophys. Res. Lett.,* **34,** doi:10.1029/2006GL028323.

Boatwright, J., 1978. Detailed spectral analysis of two small New York State earthquakes, *Bull. seism. Soc. Am.,* **68,** 1117–1131.

Chen, K.H., Bürgmann, R., Nadeau, R.M., Chen, T. & Lapusta, N., 2010. Postseismic variations in seismic moment and recurrence interval of repeating earthquakes, *Earth planet. Sci. Lett.,* **299,** 118–125.

Chen, T. & Lapusta, N., 2009. Scaling of small repeating earthquakes explained by interaction of seismic and aseismic slip in a rate and state fault model, *J. geophys. Res.,* **114,** doi:10.1029/2008JB005749.

DeMets, C., Gordon, R.G., Argus, D.F. & Stein, S., 1994. Effects of recent revisions to the geomagnetic reversal time scale on estimation of current plate motions, *Geophys. Res. Lett.,* **21,** 2191–2194.

El Hariri, M., Abercrombie, R.E., Rowe, C.A. & do Nascimento, A.F., 2010. The role of fluids in triggering earthquakes: observations from reservoir induced seismicity in Brazil, *Geophys. J. Int.*, **181,** 1566–1574.

Eshelby, J.D., 1957. The determination of the elastic field of an ellipsoidal inclusion and related problems, *Proc. R. Soc.Lond.,* **241,** 376–396.

Frankel, A. & Wennerberg, L., 1989. Microearthquake spectra from the Anza, California, seismic network: site response and source scaling, *Bull. seism. Soc. Am.,* **79,** 581–609.

Hanks, T.C. & Kanamori, H., 1979. A moment magnitude scale, *J. geophys. Res.,* **84,** 2348–2350.

Hasegawa, A., Umino, N. & Takagi, A., 1978. Double-planed structure of the deep seismic zone in the northern Japan arc, *Tectonophysics*, **47,** 43–58.

Hori, T. & Miyazaki, S., 2010. Hierarchical asperity model for multiscale characteristic earthquakes: a numerical study for the off-Kamaishi earthquake sequence in the NE Japan subduction zone, *Geophys. Res. Lett.,* **37,** L10304, doi:10.1029/2010GL042669.

Hough, S.E., 1997. Empirical Green’s function analysis: taking the next step, *J. geophys. Res.,* **102,** 5369–5384.

Ide, S., Baltay, A. & Beroza, G.C., 2011. Shallow dynamic overshoot and energetic deep rupture in the 2011 Mw 9.0 Tohoku-Oki earthquake, *Science,* **332,** 1426–1429, doi:10.1126/science.1207020.

Ide, S., Beroza, G.C., Prejean, S.G. & Ellsworth W.L., 2003. Apparent break in earthquake scaling due to path and site effects on deep borehole recordings, *J. geophys. Res.,* **108,** 10.1029/2001JB001617.

Iinuma, T. *et al*., 2012. Huge slip in small area on very shallow plate interface during M9.0 Tohoku Earthquake, *Earth planet. Sci. Lett.,* submitted

Imanishi, K. & Ellsworth, W.L., 2006. Source scaling relationships of microearthquakes at Parkfield, CA, determined using the SAFOD pilot hole seismic array, *Earthquakes: Radiated Energy and the Physics of Faulting,* Geophys. Monogr. Ser. Vol. 170, pp. 81–90, eds Abercrombie, R., McGarr, A., Kanamori, H. & Di Toro, G., American Geophysical Union, Washington, DC.

Kao, H. *et al*., 2006. Spatial-temporal patterns of seismic tremors in northern Cascadia, *J. geophys. Res.,* **111,** B03309, doi:10.1029/2005JB003727.

Kato, N., 2004. Repeating slip events at a circular asperity: numerical simulation with a rate- and state-dependent friction law, *Bull. Earthq. Res. Inst., Univ. Tokyo.,* **78**(2), 151–166.

Matsuzawa, T., Igarashi, T. & Hasegawa, A., 2002. Characteristic small-earthquake sequence off Sanriku, northeastern Honshu, Japan, *Geophys. Res. Lett.,* **29,** doi:10.1029/2001GL014632.

Nadeau R.M., Michelini, A., Uhrhammer, R.A., Dolenc, D., McEvilly T.V., 2004. Detailed kinematics, structure and recurrence of microseismicity in the SAFOD target region, *Geophys. Res. Lett.,* **31,** L12S08, doi:10.1029/2003GL019409.

Okada, T., Matsuzawa, T. & Hasegawa, A., 2003. Comparison of source areas of M4.8+/– 0.1 earthquakes off Kamaishi, NE Japan—are asperities persistent features?, *Earth planet. Sci. Lett.,* **213,** 361–374.

Okada, T., Sakoda, K., Matsuzawa, T., Hino, R., Hasegawa, A., Sakai, S. & Kanazawa, T., 2004. Characteristic seismic activity in the subducting plate boundary zone off Kamaishi, northeastern Japan, revealed by precise hypocenter distribution analysis using ocean-bottom seismometers, *Geophys. Res. Lett.,* **31,** doi:10.1029/2004GL020366.

Pollitz, F.F., Bürgmann, R. & Banerjee, P., 2011, Geodetic slip model of the 2011 M9.0 Tohoku earthquake, *Geophys. Res. Lett.,* **38,** L00G08, doi:10.1029/2011GL048632.

Poupinet, G., Ellsworth, W.L. & Frechet, J., 1984. Monitoring velocity variations in the crust using earthquake doublets: an application to the Calaveras Fault, California, *J. geophys. Res.,* **89,** 5719–5731.

Research Center for Prediction of Earthquakes and Volcanic Eruptions, 2004. Technical reports on earthquakes and volcanoes, **32**, 65.

Sato, T. & Hirasawa, T., 1973. Body wave spectra from propagating shear cracks, *J. Phys. Earth,* **21,** 415–431.

Shelly, D.R., Ellsworth, W.L., Ryberg, T., Haberland, C., Fuis, G.S., Murphy, J., Nadeau, R.M. & Bürgmann, R., 2009. Precise location of San Andreas Fault tremors near Cholame, California using seismometer clusters: Slip on the deep extension of the fault?, *Geophys. Res. Lett.,* **36,** L01303, doi:10.1029/2008GL036367.

Shimamura, K., Matsuzawa, T., Okada, T., Uchida, N., Kono, T. & Hasegawa, A., 2011. Similarities and differences in the rupture process of the M $\sim$ 4.8 repeating-earthquake sequence off Kamaishi, northeast Japan: comparison between the 2001 and 2008 events, *Bull. seism. Soc. Am.,* **101**(5), 2355–2368.

Suwa, Y., Miura, S., Hasegawa, A., Sato, T. & Tachibana, K., 2006. Interplate coupling beneath NE Japan inferred from three dimensional displacement fields, *J. geophys. Res.,* **111,** B04402, doi:101029/2004JB003203.

Tsuji, Y., Nakajima, J. & Hasegawa, A., 2008. Tomographic evidence for hydrated oceanic crust of the Pacific slab beneath northeastern Japan: implications for water transportation in subduction zones, *Geophys. Res. Lett.,* **35,** L14308, doi:10.1029/2008GL034461.

Uchida, N., Matsuzawa, T., Hasegawa, A. & Igarashi, T., 2005. Recurrence intervals of characteristic M4.8+/-0.1 earthquakes off Kamaishi, NE Japan—comparison with creep rate estimated from small repeating earthquake data, *Earth planet. Sci. Lett.,* **233,** 155–165.

Uchida, N., Matsuzawa, T., Ellsworth, W.L., Imanishi, K., Okada, T. & Hasegawa, A., 2007. Source parameters of a M4.8 and its accompanying repeating earthquakes off Kamaishi, NE Japan—implications for the hierarchical structure of asperities and earthquake cycle, *Geophys. Res. Lett.,* **34,** doi:10.1029/2007GL031263.

Ueno, T., Maeda, T., Obara, K., Asano, Y. & Takeda, T., 2010. Migration of low frequency tremors revealed from multiple array analyses in western Shikoku, Japan, *J. geophys. Res.,* **115,** doi:10.1029/2008JB006051.

Waldhauser, F. & Ellsworth, W.L., 2000. A double-difference earthquake location algorithm: method and application to the Northern Hayward fault, California, *Bull. seism. Soc. Am.,* **90,** 1353–1368.

Waldhauser, F., Ellsworth, W.L., Schaff, D.P. & Cole, A., 2004. Streaks, multiplets, and holes: high-resolution spatio-temporal behavior of Parkfield seismicity, *Geophys. Res. Lett.,* **31,** L18608, doi:10.1029/2004GL020649.

Wessel, P. & Smith, W.H.F., 1995. New version of generic mapping tools released, *EOS, Trans. Am. geophys. Un.* **79,** 329.

Yoshida, S. & Kato, N., 2003. Episodic aseismic slip in a two-degree-of-freedom block-spring model, *Geophys. Res. Lett.,* **30**(13), doi:10.1029/2003GL017439.